

Numerical study on the resonance behavior of submerged floating tunnels with elastic joint

Joohyun Park^a, Seok-Jun Kang^b, Hyun-Joong Hwang^c and Gye-Chun Cho^{*}

Department of Civil and Environmental Engineering, Korea Advanced Institute of Science and Technology,
291 Daehak-ro, Yuseong-gu, Daejeon 34141, Republic of Korea

(Received September 15, 2021, Revised February 14, 2022, Accepted March 15, 2022)

Abstract. In submerged floating tunnels (SFTs), a next-generation maritime transportation infrastructure, the tunnel module floats in water due to buoyancy. For the effective and economical use of SFTs, connection with the ground is inevitable, but the stability of the shore connection is weak due to stress concentration caused by the displacement difference between the subsea bored tunnel and the SFT. The use of an elastic joint has been proposed as a solution to solve the stability problem, but it changes the dynamic characteristics of the SFT, such as natural frequency and mode shape. In this study, the finite element method (FEM) was used to simulate the elastic joints in shore connections, assuming that the ground is a hard rock without displacement. In addition, a small-scale model test was performed for FEM model validation. A parametric study was conducted on the resonance behavior such as the natural frequency change and velocity, stress, and reaction force distribution change of the SFT system by varying the joint stiffness under loading conditions of various frequencies and directions. The results indicated that the natural frequency of the SFT system increased as the stiffness of the elastic joint increased, and the risk of resonance was the highest in the low-frequency environment. Moreover, stress concentration was observed in both the SFT and the shore connection when resonance occurred in the vertical mode. The results of this study are expected to be utilized in the process of quantitative research such as designing elastic joints to prevent resonance in the future.

Keywords: elastic joint design; finite element method; natural frequency; resonance behavior; submerged floating tunnel

1. Introduction

Traditionally, sea and air transport has been the main means of crossing the sea. However, there is a demand for alternative means of transportation because conventional methods are affected by environmental factors such as climate change. As a result, since the 1990s, the concept of a submerged floating tunnel (SFT), in which a tunnel is operated while floating in water owing to buoyancy, has been proposed, and preliminary research has been conducted (Kunish *et al.* 1994). Since the 2010s, detailed design and research, including the development of prototypes for actual construction, have been actively developed on SFTs as a next-generation marine transportation infrastructure (Jakobsen 2010). The SFT should be connected to an island or a sub-seaboard tunnel for more economical and efficient use. As the length of the SFT increases, the connection becomes essential for maintenance and risk management (Mazzolani *et al.* 2010).

The strength and stress concentration of the shore connection should be evaluated to ensure SFT stability

(Kang *et al.* 2020). However, the SFT and ground exhibit different behaviors (Nilsen and Palmstrom 2001, Shi *et al.* 2016). Displacement occurs dynamically when an SFT floating in water (Tariverdilo *et al.* 2011) is subjected to marine environmental factors, such as waves (Morita *et al.* 1994, Yan *et al.* 2016), and dynamic loads, such as traffic and earthquake loads (Jiang *et al.* 2016). However, in the case of a subsea bored tunnel surrounded by the ground, relatively small displacements are expected (Cabalar 2016, Do *et al.* 2018). Owing to this displacement difference, a problem such as stress concentration occurs in the shore connection between the SFT and bored tunnel, which considerably reduces the stability of the SFT (Chong *et al.* 2019). The use of an elastic joint has been proposed as a solution to improve the stability of shore connections by relieving the stress concentration (Kang *et al.* 2020). Even if the stress concentration is relieved by using an elastic joint, resonance behavior such as a large increase in the displacement occurs in an environment close to the natural frequency of the SFT system (Kang *et al.* 2021). Therefore, the connection between the subsea bored tunnel and the SFT should be designed considering the structural (Yarramsetty *et al.* 2019) and marine environmental characteristics of the SFT segment, as well as the resonance behavior of the SFT and the behavior of the ground.

Previous studies have mainly numerically and experimentally investigated the dynamic behavior of the SFT (Oh *et al.* 2013, Seo *et al.* 2015) under the condition of a dynamic load applied to the SFT. Although the dynamic

*Corresponding author, Professor
E-mail: gyechun@kaist.ac.kr

^aPh.D. Student

^bPh.D. Student

^cPh.D. Student

response of the SFT is affected by the boundary conditions (Jin and Kim 2017), most studies have focused only on the dynamic behavior under various dynamic loads, such as waves, traffic loads, and earthquake loads (Kunish *et al.* 1994, Hong and Ge 2010, Youshi and Fei 2010, Lee *et al.* 2017, Jin and Kim 2018), were applied at both ends of the fixed SFT. However, by using an elastic joint to resolve the stress imbalance caused by the difference in displacement between the SFT and ground in the shore connection, the SFT boundary conditions change (Kang *et al.* 2020, Kwak *et al.* 2018). Changes in these boundary conditions alter the dynamic properties, such as the natural frequency and mode shape of the structure (Lindholm *et al.* 1965, Murgan *et al.* 2016), and may cause stress concentration at the elastic boundary when resonance occurs. Although studies such as mode analysis of the SFT tether have been conducted, studies on the dynamic behavior of the SFT at the elastic boundary remain insufficient. Recently, a study was conducted on the effect of the dynamic behavior of the SFT on the behavior change of the ground, where an elastic joint was applied to the shore connection (Kang *et al.* 2020, Kang *et al.* 2021). However, this study considered only the load in the vertical direction, neglecting the dynamic behavior according to the mode shape change and fracture of the joint material. Therefore, it is necessary to study the effects of the use of an elastic joint in the shore connection between the SFT and the subsea bored tunnel on the resonance behavior of the SFT and the change in the stress distribution at the elastic boundary when the boundary conditions change.

In this study, the effect of using an elastic joint for the shore connection between the subsea bored tunnel and the SFT was analyzed using the finite element method (FEM) with a simplified liner elastic model and modes 1, 3, and 5 were mainly analyzed. The elastic joint, used to avoid the stress concentration at the shore connection (Fig. 1), was considered as the elastic boundary condition. The dynamic behavior was numerically analyzed depending on the stiffness of the elastic joint. The FEM model simulating the dynamic behavior of the SFT was validated by comparing the natural frequency obtained from the numerical model with that obtained from a small-scale model test. The direction and frequency of loads applied on the SFT were controlled as parameters to evaluate the effect of the joint stiffness on the SFT under various loading conditions. Numerical analysis in this study was performed to preliminarily investigate the effect of parameters to be considered when using elastic joints in a specific site. Therefore, a simplified condition to evaluate the effect of elastic joint was assumed. Unlike existing SFT dynamic analysis studies that consider mooring systems, the simplified FEM model assumed that dynamic loads were transmitted in the form of a trigonometric function to the free end of the module connected to the shore connection. The dynamic load was applied with various frequencies to evaluate the effect of elastic joint in the resonance behavior, rather than considering the predominant frequencies of dynamic situations (e.g., earthquake, traffic, and wave). The natural frequency of the dynamic system is affected by damping, but the damping ratio of the materials constituting

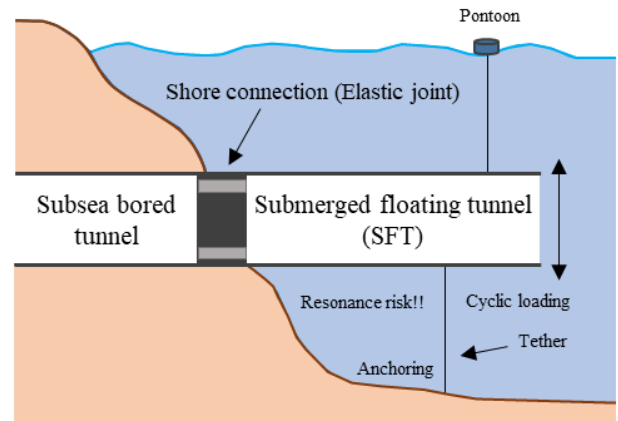


Fig. 1 Schematic diagram of elastic joint

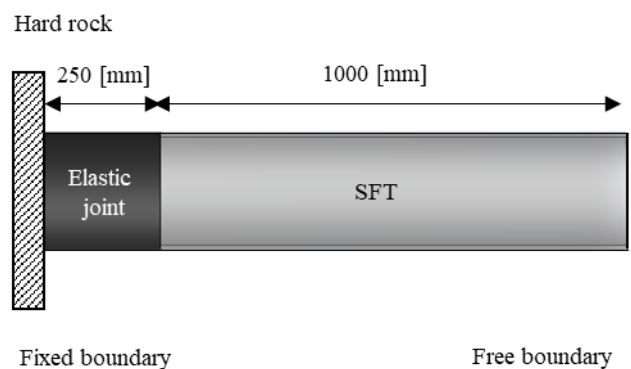


Fig. 2 FEM model

the simplified FEM model is negligibly small (Adams and Askenazi 1999, Zhu *et al.* 2007). The effect of damping was not considered to focus on the effect of elastic joint on the natural frequency of the SFT.

2. Numerical methodology

Numerical analysis based on the FEM was performed for various cases representing the effect of joint stiffness on the SFT, ground, and joint material under various loading conditions. SolidWorks (2016), developed by Dassault Systems, was used for finite element analysis. The numerical model was validated using the results of a small-scale model test.

2.1 FEM model

The FEM model consisted of an SFT module and an elastic joint. Several assumptions regarding the numerical simulation were made to focus on the dynamic behavior of the SFT considering the effect of the elastic joint: the elastic joint was fixed at one end and connected to the SFT at the other end, and the SFT, which was connected to the elastic joint at the left end, had a free boundary at the right end for application of the external loads, and damping for the entire

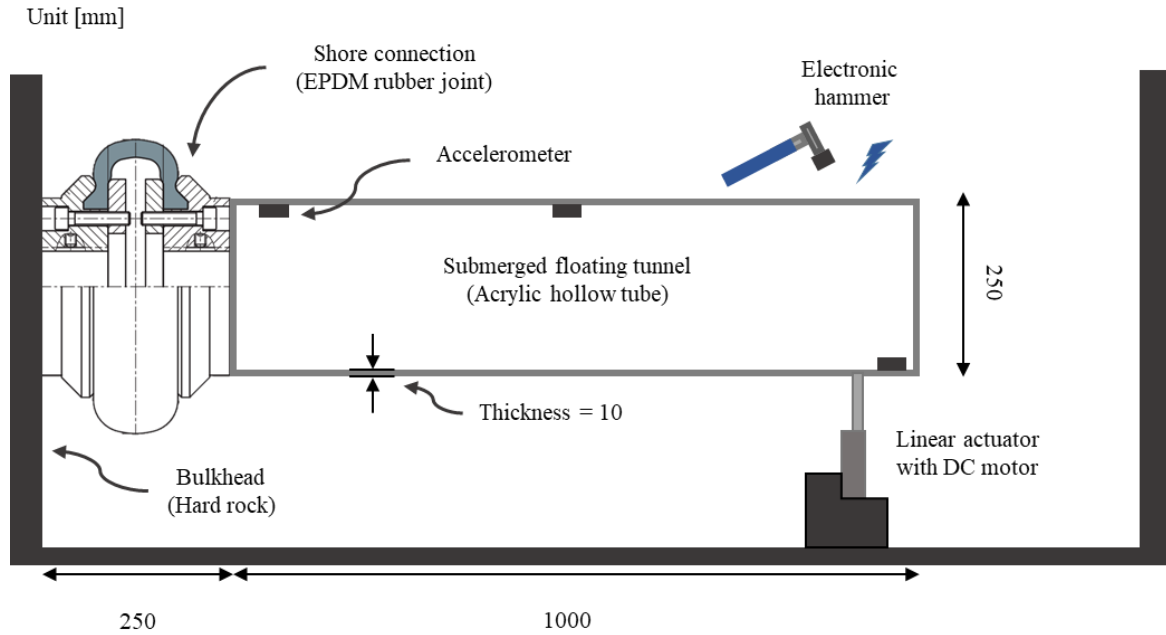


Fig. 3 Schematic diagram of small-scale model test

Table 1 Properties of small-scale SFT model

Target material	Acrylic
Density [kg/m ³]	1200
Elastic modulus [GPa]	3
Shear modulus [MPa]	890
Poisson's ratio	0.35
Tensile strength [MPa]	73
Yield strength [MPa]	45

Table 2 Properties of small-scale elastic joint

Target material	EPDM rubber
Density [kg/m ³]	960
Elastic modulus [MPa]	5
Tensile strength [MPa]	11
Poisson's ratio	0.45

Table 3 Parameters for the FEM model

Parameter	Value
Acrylic hollow tube diameter [m]	0.25
Acrylic hollow tube thickness [m]	0.01
Acrylic hollow tube length [m]	1
EPDM rubber joint diameter [m]	0.25
EPDM rubber joint thickness [m]	0.01
EPDM rubber joint length [m]	0.25
Area moment of inertia [m ²]	54.38

model was neglected. The boundary conditions of the FEM model are shown in Fig. 2. The SFT and elastic joint were assumed to be homogeneous elastic models, whose properties are presented in Tables 1 and 2, respectively. The

joint properties were determined based on the experimental results (KS M 6518) of ethylene propylene diene monomer (EPDM) rubber manufactured using the DY04303 formulation code. Elasticity models were used as the constitutive models for the FEM. Assuming that the induced response is directly proportional to the applied load, and that the load does not produce permanent deformation, a model in which the stress of an elastic material is directly proportional to the strain was employed (Tickoo 2016). The FEM model with geometric characteristics shown in Table 3 was developed to conduct validation with the small-scale model test.

The mesh size of the FEM model is strongly correlated with the frequency of the wave to be transmitted by the numerical model. In general, Kuhlmeier and Lysmer's (1973) equation is used to determine the mesh size for the accuracy of the FEM model for dynamic analysis. The equation is as follows

$$\Delta l \leq \frac{\lambda}{10}, \quad f \leq \frac{v}{10 \times \Delta l} \quad (1)$$

where Δl is the maximum mesh size, λ is the wavelength of the input motion, f is the frequency of the transmitted vibration, and v is the elastic wave velocity.

The maximum mesh size used in this numerical model was 0.0276 m, and 7568 elements and 15330 nodes were used. The shear-wave velocity calculated from the physical properties of the elastic joint used in Table 2 was 42 m/s. According to Eq. (1), energy propagation below 154 Hz is possible, confirming that the mesh size is suitable.

2.2 Small-scale model for FEM model validation

A small-scale model test is conducted to validate the FEM model. The small-scale model test consisted of a bulkhead to simulate a very hard rock that did not allow

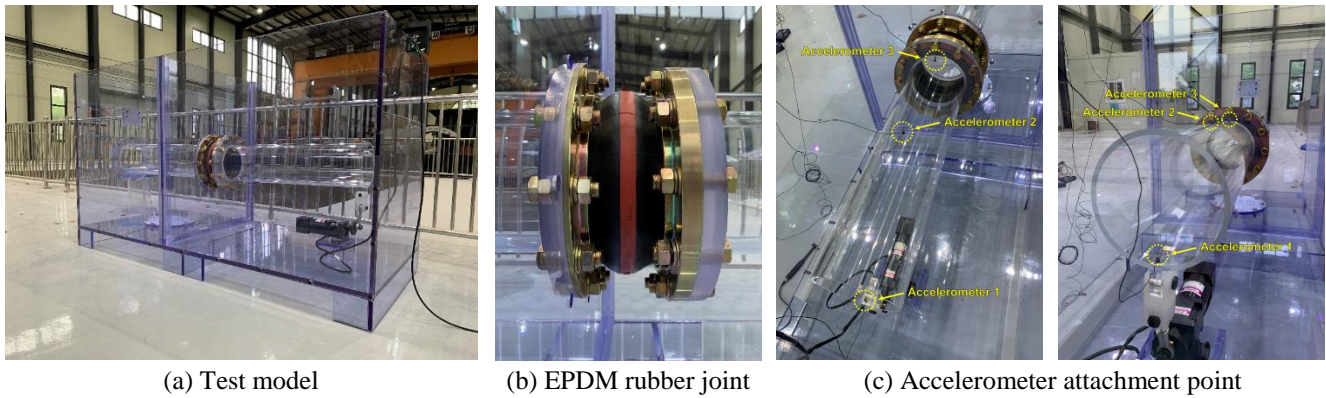


Fig. 4 Small-scale model test apparatus

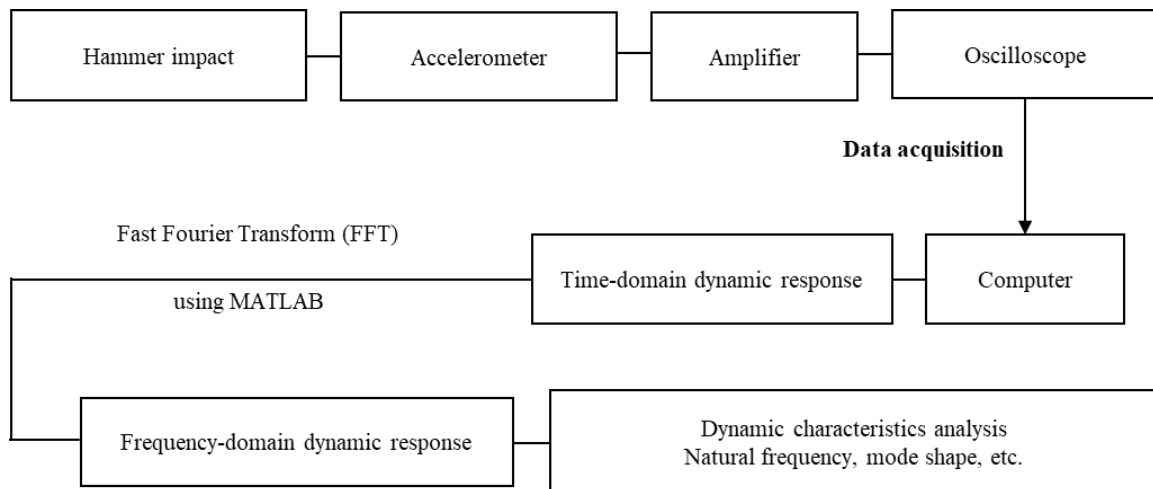


Fig. 5 Dynamic response signal processing

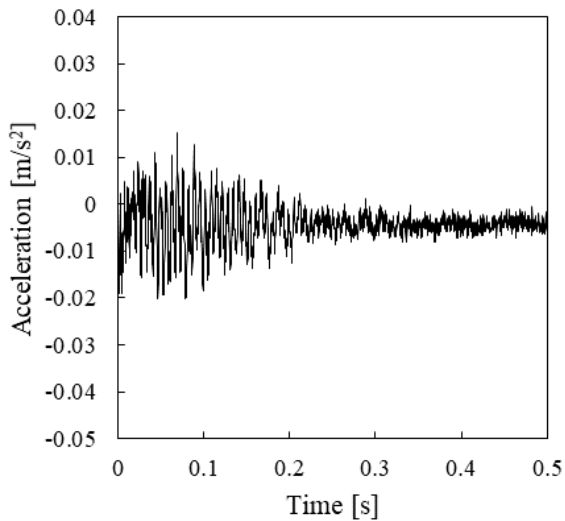
displacement, an EPDM rubber joint to simulate an elastic joint, and an acrylic hollow tube to simulate an SFT module, as shown in Fig. 3. An acrylic hollow tube and rubber joint with the same properties and parameters as those listed in Tables 1, 2, and 3 and the apparatus shown in Fig. 4, including a test model, EPDM rubber joint, and accelerometer, were used. To simulate the boundary conditions assumed in the FEM model, the bulkhead, EPDM rubber joint, and acrylic hollow tube were fixed as shown in Fig. 4(b). The dynamic response measurement system for the external impact load consisted of a PCB piezotronics electronic hammer and accelerometer, an FLC electronic pendulum instrument (amplifier), and a KEYSIGHT 4Ch 200 MHz oscilloscope. In this small-scale model test, accelerometers available from 2 Hz to 10,000 Hz and capable of measuring accelerations up to 50g were utilized to measure the dynamic response of the SFT model caused by a hammer strike. The accelerometer used in the experiment had a sensitivity of 100 mV/g and a resonance frequency of 25 kHz; three accelerometers were vertically attached, as shown in Fig. 4(c), to measure the response in the vertical direction to observe the effect of the measurement position.

The time-domain dynamic response acquired by the accelerometers was analyzed through signal processing, as

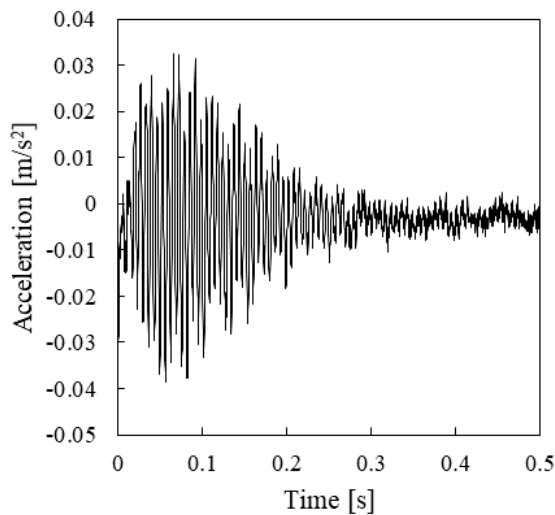
shown in Fig. 5. The time-domain dynamic response must be converted into a frequency-domain dynamic response to analyze dynamic characteristics, such as natural frequency and mode shape. Signal processing to transform time-domain signals into frequency-domain signals was performed in MATLAB using a fast Fourier transform (FFT) algorithm. The noise in the time-domain dynamic response results was removed using 1) a low-pass filter that attenuated signals with frequencies above a specific cut-off frequency and passed only frequency signals below the cut-off frequency, and 2) a high-pass filter algorithm that passed only frequency signals above the cut-off frequency. This signal processing was used to analyze the test results of the small-scale model and the response when an impact load was applied to the FEM model. The most dominant frequency in the frequency-domain dynamic response after the signal processing was evaluated as the natural frequency (Doebeling *et al.* 1998).

2.3 FEM model validation

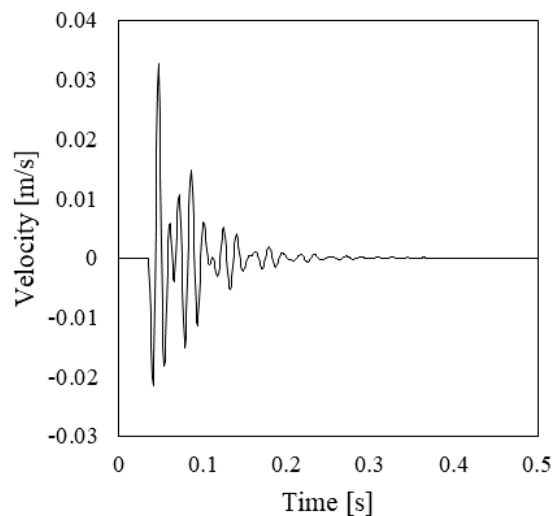
Although the SFT had a free boundary at the right end of the FEM model, a linear actuator with a direct current (DC) motor to apply a cyclic load was fixed to the end of the acrylic hollow tube in a small-scale model test



(a) Small-scale model test (Accelerometer 3)



(b) Small-scale model test (Accelerometer 2)



(c) FEM model

Fig. 6 Time-domain dynamic response

apparatus. Therefore, the results of the small-scale model tests were compared with those of the FEM model with an SFT having a fixed boundary at the right end. In addition, like the small-scale model test, the time-domain responses obtained after applying an impact load to the SFT of the FEM model were compared.

Displacement, velocity, and acceleration can be used to determine the amplitude of the vibration that occurs when an external force is applied to the system. They have different magnitudes and phases but the same frequency. As shown in Fig. 6, the amplitude of the time-domain response owing to the impact load decreases with time. Because the structure vibrates at a natural frequency (Chopra, 2012), the natural frequency of the SFT system using elastic joints can be determined through transient response analysis. Fig. 6(a) and Fig. 6(b) show the time-domain acceleration response results obtained from accelerometers attached to different positions in the small-scale model test, and Fig. 6(c) shows the time-domain velocity response measured in the FEM model. The first significant response owing to the impact load and response to free vibration was observed in both results. FFT was performed to convert the time-domain response obtained from the initial signal before the free vibration into a frequency-domain response. To remove the response due to noise, a low-pass filter of 100 Hz and a high-pass filter of 2 Hz were used in the signal processing, and the resonance frequency of the small-scale model system was obtained. The responses obtained from the accelerometers attached at intervals of 50 cm had the same natural frequency for vertical mode as 39.1 Hz. To validate the FEM model, the damping ratio was determined using the logarithmic decrement method from the response of the small-scale model test. The natural frequency for vertical mode of the FEM model was determined using the same signal processing, and its value was 40.3 Hz. Consequently, the natural frequencies for vertical mode of the small-scale model system and the FEM model were determined, as shown in Fig. 7. The dynamic characteristics derived from the experimental study were reflected well in the FEM model. The results of the natural frequency and resonance of the SFT obtained from the validated numerical model are expected to be reliable.

2.4 Case configuration for parametric study

The external load condition and stiffness of the elastic joint were the main factors in the FEM simulation, as listed in Table 4. The cases were classified into vertical, axial, and torsional directions to analyze the effect of the external load direction, the definitions of which are shown in Fig. 8. To analyze the effects of stiffness on the elastic joint, 10 stiffness cases were set at equal intervals between 1 and 10 MPa, centered at 5 MPa, which is the stiffness of the elastic joint of the small-scale model test used for validation of the FEM model. To perform the resonance behavior analysis of the SFT system using the elastic joint, eight cyclic load with frequencies ranging from 1 Hz to 30 Hz were selected, and parametric studies were performed on the SFT system.

A parametric study through FEM simulation was performed to analyze the natural frequency according to the direction of the external impact load, dynamic behavior

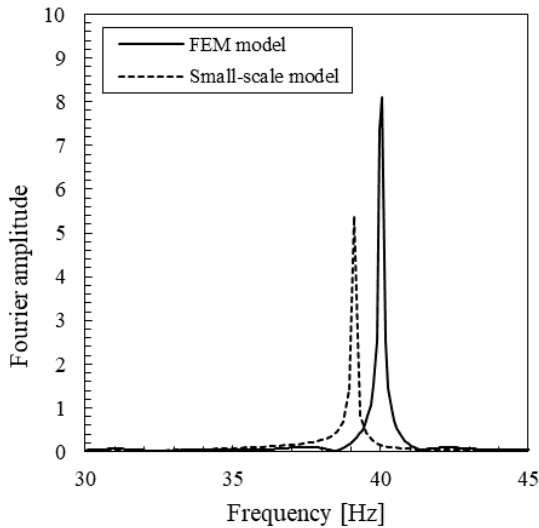


Fig. 7 Frequency-domain dynamic response of FEM and small-scale models

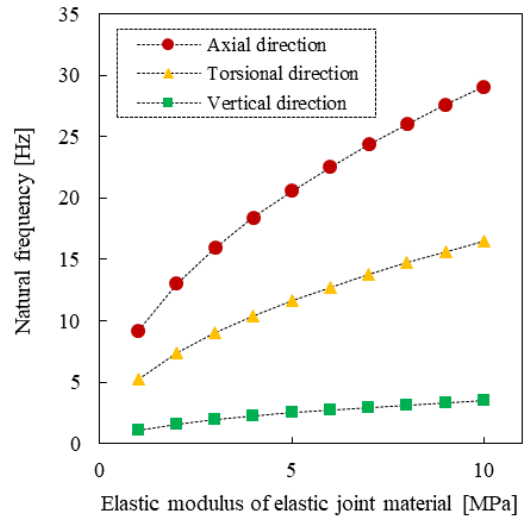


Fig. 9 Relationship between elastic modulus of elastic joint and natural frequency of SFT

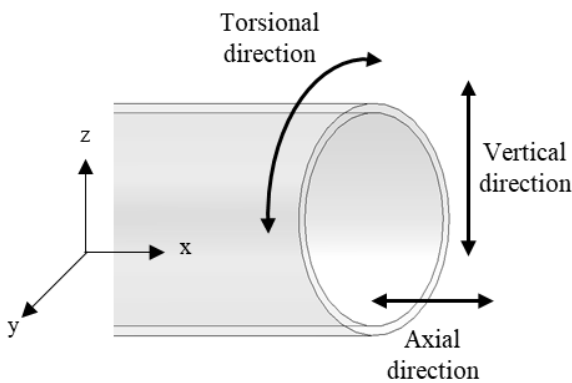


Fig. 8 Load directions

Table 4 FEM simulation cases

Direction of external load	Vertical direction
	Axial direction
	Torsional direction
Cyclic loading frequency [Hz]	1, 2, 3, 5, 10, 15, 20, 30
Elastic modulus of joint [MPa]	10 cases from 1 to 10

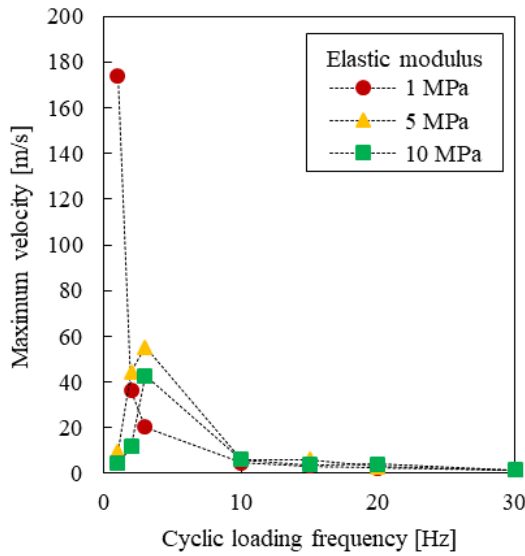
according to the cyclic loading frequency, and dynamic behavior according to the stiffness of the elastic joint. The natural frequency was determined by the signal processing of the dynamic response obtained by applying impact loads to the SFT in the vertical, axial, and torsional directions. Furthermore, the risk of failure according to the load characteristics was assessed by analyzing the stress distribution of the SFT and elastic joints according to the load characteristics. Thus, the maximum velocity and maximum stress of the SFT, maximum stress of the elastic joint material, and maximum reaction force at the elastic boundary were analyzed at various loading frequencies in each load direction.

3. Dynamic behavior of SFT

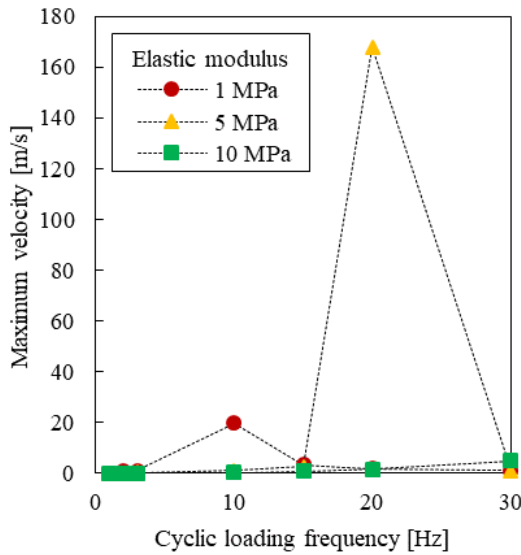
3.1 Natural frequency with three mode shapes

In this study, modal analysis was performed using SolidWorks 2016, which was used as the finite element analysis software. The results confirmed that the vertical, torsional, and axial behaviors were dominant in Modes 1, 3, and 5, respectively. Therefore, these three modes were analyzed as the main targets. For the three mode shapes in the vertical, axial, and torsional directions, the natural frequencies of the SFT were investigated based on the stiffness of the elastic joint. Fig. 9 shows the natural frequency values for each mode shape depending on the elastic joint stiffness. The results indicate that the natural frequency of the SFT increased as the stiffness of the elastic joint increased in all modes. The natural frequencies were large in the order of axial, torsional, and vertical mode shapes.

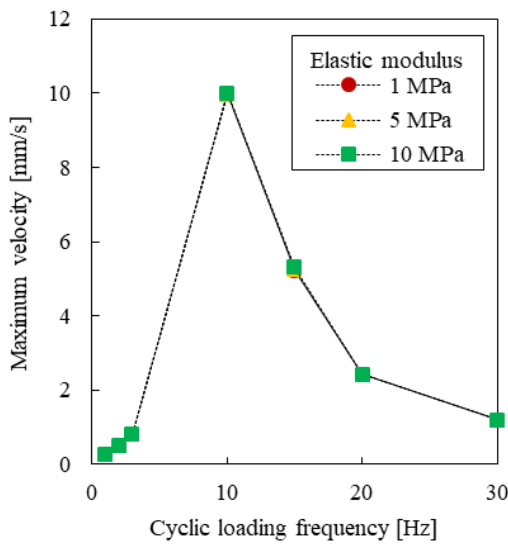
In general, the vibration characteristics measured during the stability evaluation of structures using natural frequencies exhibit a larger change in the higher-order mode (Fritzen 2005). It was confirmed that this trend also appeared in an SFT system in which elastic joints were used. In addition, as the stiffness of the elastic joint increases, the natural frequency increases the most in the axial mode shape. Therefore, the axial mode shape is the most sensitive to changes in the elastic modulus, which must be considered when designing the corresponding elastic joint. To alternatively express the natural frequency of the SFT system under fixed-end conditions, modal analysis was performed by applying a significantly high elastic modulus to the elastic joint material. Consequently, it was confirmed that the reference natural frequency had values of 68 Hz in the vertical mode, 148 Hz in the torsional mode, and 205 Hz in the axial mode. The natural frequency for each mode tends to increase as the joint stiffness increases in the form of a power function, and is



(a) Vertical cyclic load



(b) Axial cyclic load



(c) Torsional cyclic load

Fig. 10 Maximum velocity of SFT according to frequency under different cyclic load directions

expected to converge to the value of the fixed-end condition.

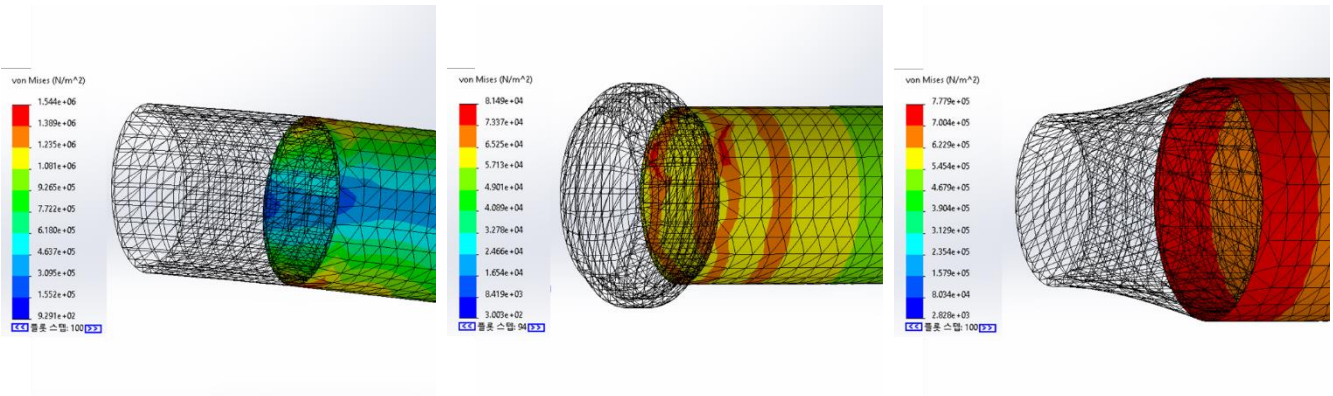
3.2 Amplified velocity of SFT with resonance

The effects of joint stiffness and loading characteristics on the change in the maximum velocity of the SFT were analyzed using a parametric study. The results were obtained in the vertical, axial, and torsional directions as shown in Fig. 10. The results showed that when a vertical cyclic load was applied in a low-frequency environment and when an axial cyclic load was applied in a relatively high-frequency environment (Fig. 10(b)), they had large maximum velocities. When a vertical cyclic load is applied, an elastic joint with a softer elastic modulus is used when the maximum velocity is higher. In an elastic joint with an elastic modulus of 1 MPa, the natural frequency of the mode shape in the vertical direction was approximately 1 Hz, as shown in Fig. 9. As a result, resonance occurred spontaneously in the 1-Hz environment. In the axial mode shape, the natural frequency of the joint with an elastic modulus of 5 MPa was approximately 20 Hz. Therefore, resonance occurred in a close 20-Hz environment. Regardless of the stiffness of the elastic joint, the same tendency was observed when a load was applied in the torsional direction. The FEM model did not consider the torsional stiffness. Even if an elastic joint with the same stiffness is used, the frequency band in which resonance occurs varies according to the applied load direction. This indicates that the effect of each element on the load should be considered when designing an elastic joint.

3.3 Stress distribution on SFT with resonance

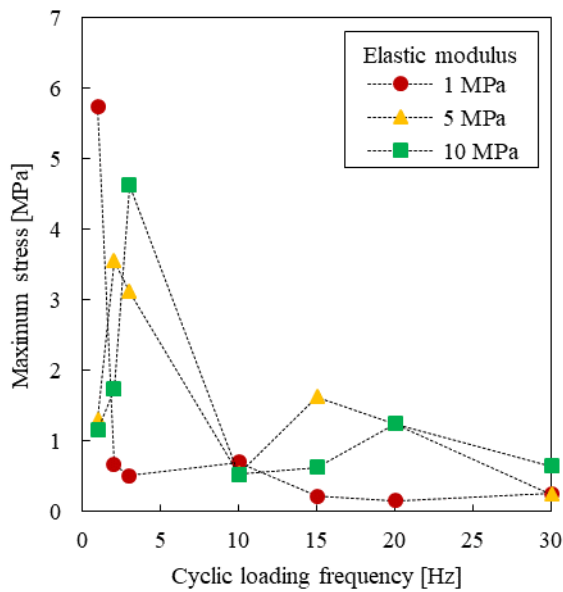
The effects of these factors on the stress occurring in the SFT were analyzed and compared using a parametric study. The stress distributions of the SFT in the presence of cyclic loads in the vertical, axial, and torsional directions are shown in Fig. 11. When a load was applied vertically, a narrow and symmetrical vertical stress concentration occurred near the interface between the elastic joint and SFT, as shown in Fig. 11(a). When an axial load was applied, a ring-shaped stress distribution occurred near the interface between the elastic joint and SFT, as shown in Fig. 11(b). When a load was applied in the torsional direction, the stress was equally distributed around the interface between the elastic joint and SFT, as shown in Fig. 11(c).

Fig. 12 shows the magnitude of the maximum stress of the SFT according to the frequency of the cyclic load. As shown in Fig. 12(a), the magnitude of the maximum stress increases in a low-frequency environment in the case of a mode shape in the vertical direction. When an elastic joint with a low elastic modulus was used, the magnitude of the maximum stress amplified by resonance in the SFT increased. In the case of the mode shape in the axial direction, the magnitude of the maximum stress was largest in the high-frequency environment (Fig. 12 (b)). Although a larger stress occurs under an axial cyclic load, as shown in Fig. 12, if resonance occurs in a vertical mode shape in an environment consistent with the natural frequency, the

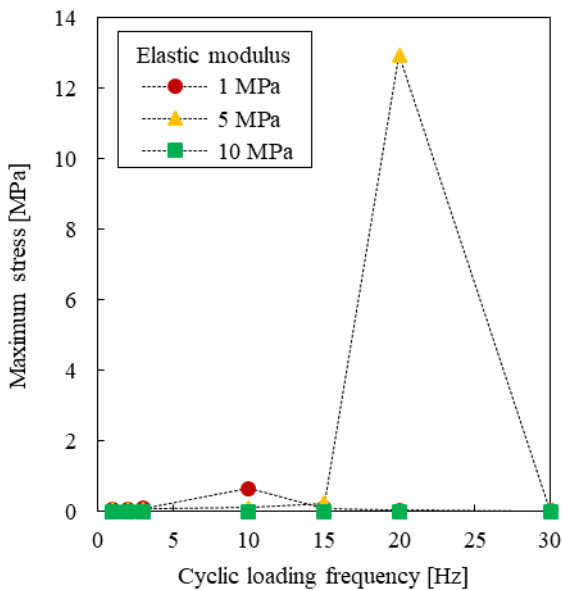


(a) Vertical cyclic load (b) Axial cyclic load (c) Torsional cyclic load

Fig. 11 Stress distribution of SFT according to the load direction



(a) Vertical cyclic load



(b) Axial cyclic load

Fig. 12 Maximum stress of SFT according to the frequency of the cyclic load

stress is concentrated in a narrow area, and the risk of SFT failure is high. This suggests that the elastic joint should be carefully designed, particularly when the target area in which the SFT is to be constructed has a low natural frequency.

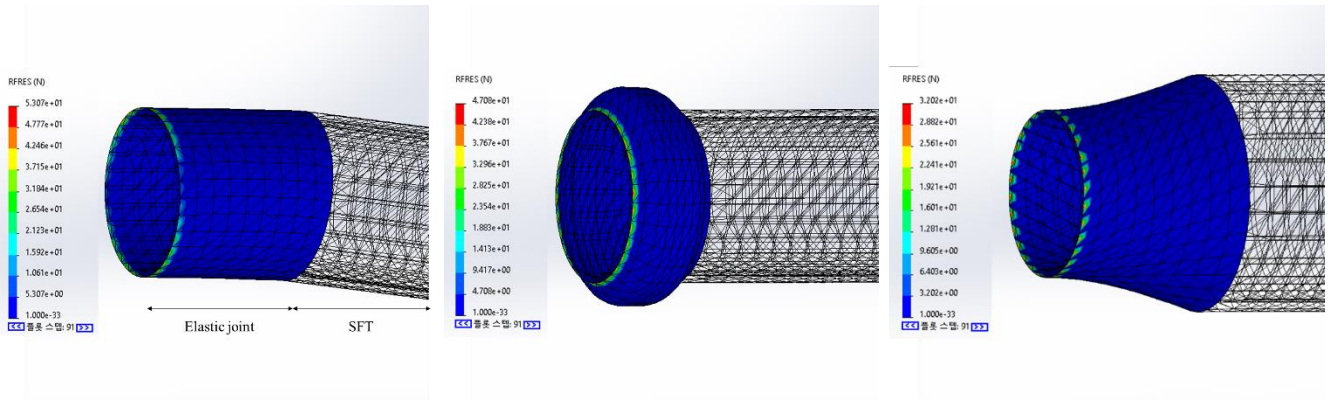
4. Dynamic behavior of shore connection

The ground and elastic joints were affected by the dynamic behavior of the SFT at the shore connection. As the ground was assumed to be an extremely hard rock that could not be moved in this FEM model, the boundary condition of the elastic joint was fixed at one end. The magnitude of the force transferred to the ground, which is the reaction force generated at the fixed end, decreases as the ground moves together when modeling the actual ground. However, to simplify the finite element analysis by minimizing the situational factor, the force applied to the fixed ground was analyzed.

4.1 Dynamic load transferred to the ground

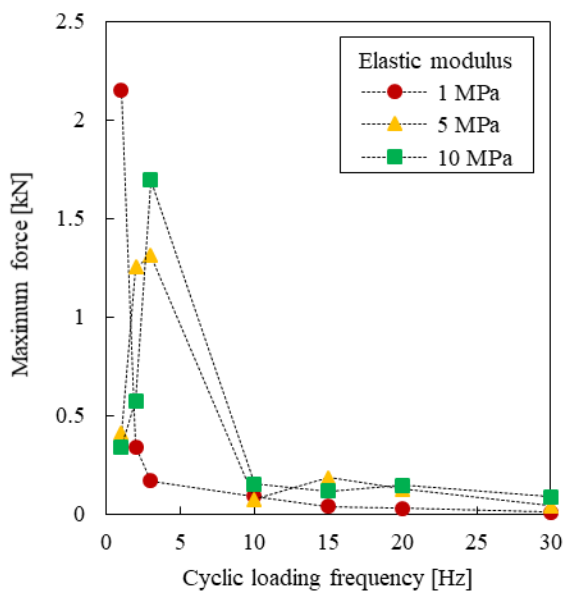
Parametric studies were conducted to investigate the effects of various factors on the change in the maximum force at the elastic boundary. Fig. 13 shows the reaction force distribution at the elastic boundary under cyclic loads in the vertical, axial, and torsional directions. As shown in Fig. 13(a), when a vertical load is applied, a narrow and symmetrical normal stress concentration is formed at the elastic boundary. When an axial load is applied, stress concentration occurs at the elastic boundary in the form of a thin ring, as illustrated in Fig. 13(b). The stress distribution when a load was applied in the torsional direction showed a stress concentration centered at the elastic boundary and spread in the torsional direction, as illustrated in Fig. 13(c).

Fig. 14 shows the magnitude of the maximum force at the elastic boundary according to the frequency of the cyclic load. Fig. 14(a) shows that the magnitude of the maximum force increased in the low-frequency loading condition when it had a vertical mode shape. When an elastic joint with a lower elastic modulus was used, the magnitude of the maximum reaction force amplified owing to the resonance increased. This means

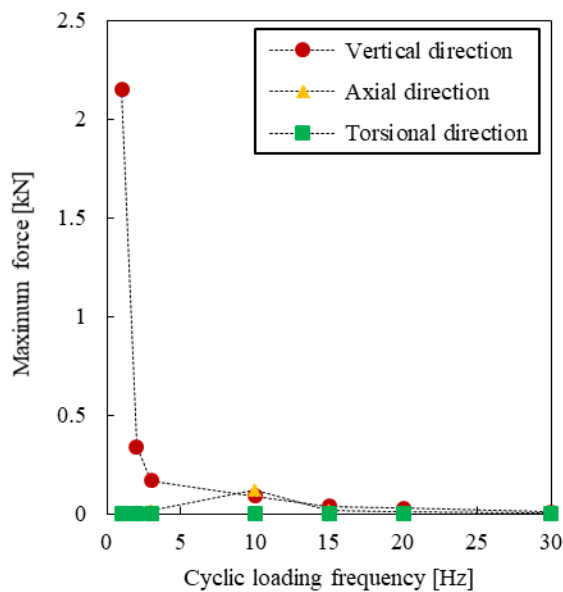


(a) Vertical cyclic load (b) Axial cyclic load (c) Torsional cyclic load

Fig. 13 Distribution of reaction force at elastic boundary according to the load direction



(a) Change in stiffness of elastic joint under vertical load



(b) Change in direction of load at 1 MPa

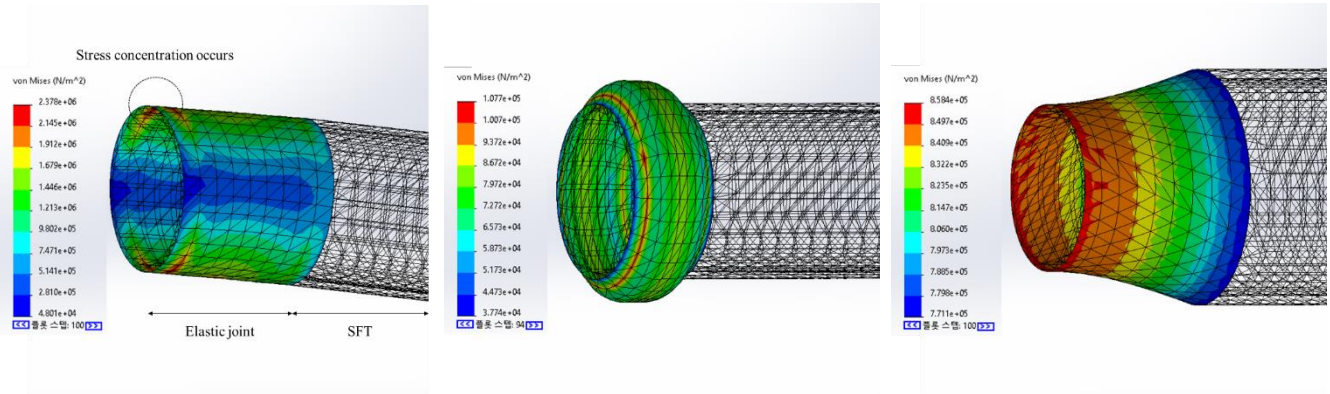
Fig. 14 Maximum force at elastic boundary according to the frequency of the cyclic load

that if resonance occurs, the magnitude of the force transmitted to the ground is large when the target area where the SFT is to be constructed has a low natural frequency. In addition, as shown in Fig. 14(b), the reaction force was the greatest when a load in the vertical direction was applied. This implies that a large force is transmitted when resonance occurred in a vertical mode shape. Therefore, when connecting an SFT to soft ground, the elastic joint should be designed with special attention to the occurrence of resonance in the vertical direction.

4.2 Stress distribution on joint with resonance

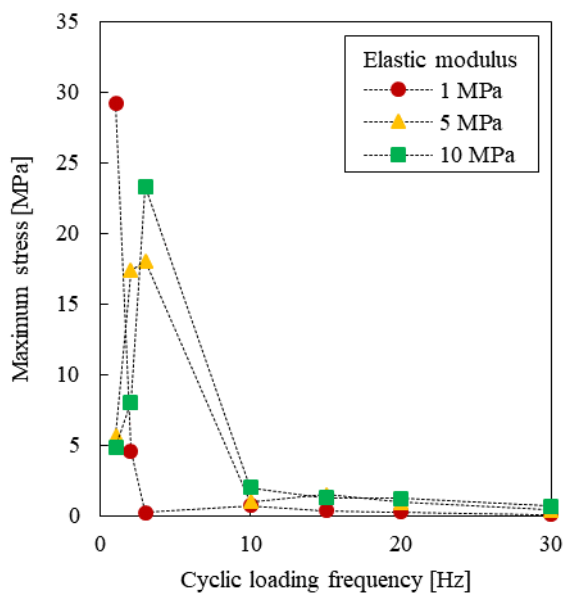
The results of the parametric studies were used to investigate the effects of various factors on the maximum stress occurring in the elastic joint material. Fig. 15 shows the stress distribution of the elastic joint material under cyclic loads in the vertical, axial, and torsional directions. When a vertical load was applied, the elastic boundary exhibited a narrow and symmetrical normal stress concentration, as shown in Fig. 15(a). As demonstrated in Fig. 15(b), when an axial load is applied, stress concentration occurs in the form of a narrow ring near the elastic boundary. The stress distribution demonstrated that, when a load was applied in the torsional direction, the stress was concentrated and spread around the elastic boundary, as illustrated in Fig. 15(c).

Fig. 16 shows the magnitude of the maximum stress in the elastic joint according to the frequency of the cyclic load. Fig. 16(a) shows that the magnitude of the maximum force increased in the low-frequency loading condition when it had a vertical mode shape. When an elastic joint with a lower elastic modulus was used, the magnitude of the maximum stress increased significantly owing to resonance. This result indicates that a significant amount of stress is generated in the elastic joint at a low natural frequency. In addition, as shown in Fig. 16(b), when a load is applied in the vertical direction, it experiences a large stress. This means that a large stress concentration occurs in a narrow area when resonance occurs in the vertical mode. Therefore, when considering the fracture of the joint material in the design of an elastic joint, it is important to avoid resonance in the vertical mode.

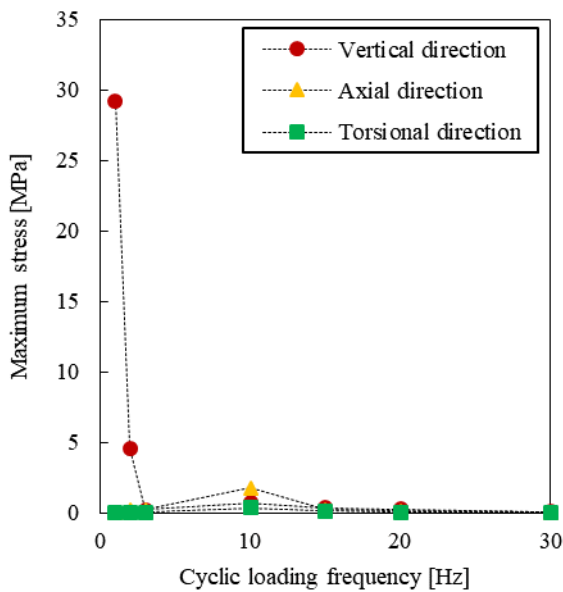


(a) Vertical cyclic load (b) Axial cyclic load (c) Torsional cyclic load

Fig. 15 Stress distribution of elastic material according to the load direction



(a) Change in stiffness of elastic joint under vertical load



(b) Change in direction of load at 1 MPa

Fig. 16 Maximum stress of joint material according to the frequency of the cyclic load

5. Conclusions

In this study, an FEM simulation was performed to analyze the natural frequency change and resonance behavior of the SFT system with an elastic joint. The FEM model used in this simulation was validated through a small-scale model test. The influence of elastic joint stiffness and external load characteristics (i.e., loading frequency and loading direction) on the SFT, ground, and elastic joint material was qualitatively analyzed. The findings of this study can be summarized as follows:

- As the stiffness of the elastic joint increased, the natural frequency of the SFT system increased in the form of a power function in all three modes of the vertical, axial, and torsional directions. This value eventually converges to the natural frequency value under the fixed-end condition.
- The rate of change in the natural frequency of the SFT system according to the stiffness change of the elastic joint was the highest in the axial mode and smallest in the vertical mode.
- When repetitive loads in the vertical direction were applied, narrow and symmetrical vertical stress concentrations appeared at the SFT and elastic boundary, whereas stress was distributed in a ring shape when repeated loads in the axial and torsional directions were applied.
- While under cyclical loading in the axial and torsional directions, a relatively uniform reaction force distribution occurred at the interface between the elastic joint and the ground, it was confirmed that a large force is transmitted to the ground in a limited and symmetrical area during repeated loads in the vertical direction.
- It was confirmed that the resonance behavior in an environment with a loading frequency similar to the natural frequency of the SFT system causes a large velocity increase and stress concentration, especially in the vertical mode.
- When designing the stiffness of the elastic joint to avoid resonance, it is possible to prevent unexpected resonance by considering two adjacent modal shapes simultaneously, and the fracture of the joint material must be considered.
- This study provides only qualitative results on the natural frequency change and resonance behavior of the SFT

system through a simplified numerical model. However, it is expected that it can be utilized in future studies by supplementing it with real-scale experiments, which include scaled-up and water confinement effects, and detailed dynamic load characteristics.

Acknowledgments

This work was supported by the National Research Foundation of Korea (NRF) grant funded by the Korea government (MSIT) (No. 2017R1A5A1014883). The first author is supported by the Innovated Talent Education Program for Smart City from MOLIT.

References

- Cabalar, A.F. (2016), "Cyclic behavior of various sands and structural materials interfaces", *Geomech. Eng.*, **10**(1), 1-19. <https://doi.org/10.12989/gae.2016.10.1.001>.
- Chong, S.H., Shin, H.S. and Cho, G. C. (2019), "Numerical analysis of offshore monopile during repetitive lateral loading", *Geomech. Eng.*, **19**(1), 79-91. <https://doi.org/10.12989/gae.2019.19.1.079>.
- Chopra, A.K. (2012), *Dynamics of structures (4th ed.)*, Pearson, New York, NY, USA.
- Cifuentes, C., Kim, S., Kim, M.H., and Park, W.S. (2015), "Numerical simulation of the coupled dynamic response of a submerged floating tunnel with mooring lines in regular waves", *Ocean Syst. Eng.*, **5**(2), 109-123. <https://doi.org/10.12989/ose.2015.5.2.109>.
- Do, N.A., Dias, D. and Oreste, P. (2018), "Numerical investigation of segmental tunnel linings-comparison between the hyperstatic reaction method and a 3D numerical model", *Geomech. Eng.*, **14**(3), 293-299. <https://doi.org/10.12989/gae.2018.14.3.293>.
- Doebling, S.W., Farrar, C.R. and Prime, M.B. (1998), "A summary review of vibration-based damage identification methods", *Shock Vib. Digest*, **30**(2), 91-105.
- Fritzen, C.P. (2005), "Vibration-based structural health monitoring-concepts and applications", *Key Eng. Mater.*, **293**, 3-20. <https://doi.org/10.4028/www.scientific.net/KEM.293-294.3>.
- Hong, Y. and Ge, F. (2010), "Dynamic response and structural integrity of submerged floating tunnel due to hydrodynamic load and accidental load", *Proc. Eng.*, **4**, 35-50. <https://doi.org/10.1016/j.proeng.2010.08.006>.
- Jakobsen, B. (2010), "Design of the Submerged Floating Tunnel operating under various conditions", *Proc. Eng.*, **4**, 71-79. <https://doi.org/10.1016/j.proeng.2010.08.009>.
- Jin, C. and Kim, M. (2017), "Dynamic and structural responses of a submerged floating tunnel under extreme wave conditions", *Ocean Syst. Eng.*, **7**(4), 413-433. <https://doi.org/10.12989/ose.2017.7.4.413>.
- Jin, C. and Kim, M.H. (2018), "Time-domain hydro-elastic analysis of a SFT (submerged floating tunnel) with mooring lines under extreme wave and seismic excitations", *Appl. Sci.*, **8**(12), 2386. <https://doi.org/10.3390/app8122386>.
- Kang, S.J., Kim, J.T. and Cho, G.C. (2020), "Preliminary study on the ground behavior at shore connection of submerged floating tunnel using numerical analysis", *Geomech. Eng.*, **21**(2), 133-142. <https://doi.org/10.12989/gae.2020.21.2.133>.
- Kang, S.J., Park, J. and Cho, G.C. (2021), "Numerical Study on Dynamic Response of Submerged Floating Tunnel Depending on Shore Connection", *Proceedings of the 2021 World Congress on Advances in Structural Engineering and Mechanics (ASEM21)*, Seoul, Korea, August. <https://doi.org/10.12989/gae.2020.21.2.133>.
- Kim, S., Kim, M.H. and Park, W.S. (2015), "Numerical simulation of the coupled dynamic response of a submerged floating tunnel with mooring lines in regular waves", *Ocean Syst. Eng.*, **5**(2), 109-123. <https://doi.org/10.12989/ose.2015.5.2.109>.
- Kuhlemeyer, R.L. and Lysmer, J. (1973), "Finite element method accuracy for wave propagation problems", *J. Soil Mech. Found.*, **99**(5), 421-427. <https://doi.org/10.1061/JSFEAQ.0001885>.
- Kunisu, H., Mizuno, S., Mizuno, Y. and Sacki, H. (1994), "Study on submerged floating tunnel characteristics under the wave condition", *Proceedings of the 4th International Offshore and Polar Engineering Conference*, Osaka, Japan, April.
- Kwak, C., Jang, D., You, K. and Park, I. (2018), "Dynamic response on tunnel with flexible segment:", *Geomech. Eng.*, **15**(3), 833-839. <https://doi.org/10.12989/gae.2018.15.3.833>.
- Lee, J.Y., Jin, C. and Kim, M. (2017), "Dynamic response analysis of submerged floating tunnels by wave and seismic excitations", *Ocean Syst. Eng.*, **7**(1), 1-19. <https://doi.org/10.12989/ose.2017.7.1.001>.
- Lindholm, U.S., Kana, D.D., Chu, W.H. and Abramson, H.N. (1965), "Elastic vibration characteristics of cantilever plates in water", *J. Ship Prod. Des.*, **9**(02), 11-36. <https://doi.org/10.5957/jsr.1965.9.2.11>.
- Mazzolani, F.M., Faggiano, B. and Martire, G. (2010), "Design aspects of the AB prototype in the Qiandao Lake", *Proc. Eng.*, **4**, 21-33. <https://doi.org/10.1016/j.proeng.2010.08.005>.
- Morita, S., Yamashita, T., Mizuno, Y., Mineta, M. and Kurosaki, K. (1994), "Earthquake Response Analysis of Submerged Floating Tunnels Considering Water Compressibility", *Proceedings of the 4th International Offshore and Polar Engineering Conference*, Osaka, Japan, April.
- Murugan, R., Ramesh, R. and Padmanabhan, K. (2016), "Investigation of the mechanical behavior and vibration characteristics of thin walled glass/carbon hybrid composite beams under a fixed-free boundary condition", *Mech. Adv. Mater. Struct.*, **23**(8), 909-916. <https://doi.org/10.1080/15376494.2015.1056394>.
- Nilsen, B., & Palmstrøm, A. (2017), "Stability and water leakage of hard rock subsea tunnels", *Modern Tunn. Sci. Technol.*, 497-502.
- Oh, S.H., Park, W.S., Jang, S.C. and Kim, D.H. (2013), "Investigation on the behavioral and hydrodynamic characteristics of submerged floating tunnel based on regular wave experiments", *J. Kor. Soc. Civ. Eng.*, **33**(5), 1887-1895. <https://doi.org/10.12652/Ksce.2013.33.5.1887>.
- Seo, S.I., Mun, H.S., Lee, J.H. and Kim, J.H. (2015), "Simplified analysis for estimation of the behavior of a submerged floating tunnel in waves and experimental verification", *Mar. Struct.*, **44**, 142-158. <https://doi.org/10.1016/j.marstruc.2015.09.002>.
- Shi, P., Zhang, D., Pan, J. and Liu, W. (2016), "Geological investigation and tunnel excavation aspects of the weakness zones of Xiang'an subsea tunnels in China", *Rock Mech. Rock Eng.*, **49**(12), 4853-4867. <https://doi.org/10.1007/s00603-016-1076-z>.
- Tariverdilo, S., Mirzapour, J., Shahmardani, M., Shabani, R. and Gheyretmand, C. (2011). "Vibration of submerged floating tunnels due to moving loads", *Appl. Math. Model.*, **35**(11), 5413-5425. <https://doi.org/10.1016/j.apm.2011.04.038>.
- Tickoo, S. (2016), *SolidWorks 2016 for Designers*, CAD/CIM Technologies, Schererville, IN, USA.
- Yan, H., Luo, Y. and Yu, J. (2016), "Dynamic response of submerged floating tunnel in the flow field", *Proc. Eng.*, **166**, 107-117. <https://doi.org/10.1016/j.proeng.2016.11.573>.
- Yarramsetty, P.C.R., Domala, V., Poluraju, P. and Sharma, R.

- (2019), "A study on response analysis of submerged floating tunnel with linear and nonlinear cables", *Ocean Syst. Eng.*, **9**(3), 219-240. <https://doi.org/10.12989/ose.2019.9.3.219>.
- Youshi, H. and Fei, G. (2010), "Dynamic response and structural integrity of submerged floating", *Proc. Eng.*, **4**, 35-50. <https://doi.org/10.1016/j.proeng.2010.08.006>.